12th Brazilian Congress of Manufacturing Engineering
May 10th-12th, 2023, Brasilia, DF, Brazil

ANALYSIS OF THE MECHANICAL PROPERTIES OF PH1 STAINLESS STEEL COMPONENTS MANUFACTURED THROUGH DMLS

Renan Ferreira Fraga Wanderley
Jaime Tupiassú Pinho de Castro
Felipe de Castro Gouvea
Pontifical Catholic University of Rio de Janeiro; Rio de Janeiro/Brazil
renanf@puc-rio.br; jtcastro@puc-rio.br; fgouvea@puc-rio.br

Abstract. *Advanced manufacturing, more specifically additive manufacturing, has been increasingly explored since the emergence of the so-called Industry 4.0. 3D printing techniques, including the great diversity of technologies and materials that can be used, allow a wide range of applications. In order to further explore and deepen the studies related to this topic, this research investigated the mechanical properties of PH1 stainless steel, manufactured in an EOS M280 printer through the Direct Metal Laser Sintering process, or DMLS for short. The characteristics of the material were explored, identifying influences of the form of manufacture and comparing its measured properties with those reported by the printer manufacturer and with similar laminated materials found on the market. Different printing orientations were analyzed, in addition to the difference between parts produced with and without heat treatment, which is recommended by the manufacture because parts manufactured by this method contain a high amount of residual stress. The tensile, roughness, hardness, impact tests and the SEM analysis were selected considering obtaining the most relevant properties of the material for the industry of the parts produced by the technology. The measured results were compared with those obtained by traditional manufacturing, so that it was possible to analyze the feasibility and reliability of replacing the manufacturing method. These indicate that the printed material is resistant and can replace parts obtained by traditional manufacturing, but it must be used with some care, as it is very much affected by the printing orientation, showing very different results appearing in some cases to be even different materials. Additionally, a script for the digital manufacturing of spare parts, considering different scenarios, was developed, to allow the manufacture of parts that, together with the mechanical tests performed, allows the evaluation of the path to be followed within the additive manufacturing for each part.*

Keywords: *Mechanical Properties; Additive Manufacturing; PH1 Stainless Steel; 3D Printing; Digital Manufacturing*

1. INTRODUCTION

The Brazilian industry, and in particular the oil and gas sector, is facing a new window of opportunity with the transformations of the fourth wave of the Industrial Revolution, the so-called Industry 4.0. The traditional manufacturing industry is at the start of an accelerated digital transformation, through the adoption of technologies such as intelligent robots and sensors, autonomous drones, 3D printing, among other innovative technologies. This transformation can be compared to the automation of production in the early 1970s, which substantially increased the productivity of the industry. Today, the association of information and communication technologies is allowing a true innovative approach in all production chains, within a growing process of digitization (Bosch, 2021).

Considering the rapid technological advances involving Industry 4.0, and the consequent need for digital transformation of companies, additive manufacturing has been gaining ground and generating new challenges for engineering. One of the main challenges is the need for transition and change in conception, in the development of new products, and in the manufacture of goods, where the mental model based on traditional manufacturing will pass gradually to the model based on additive manufacturing and other digital manufacturing techniques. However, it turns out that this transition has been happening in practice more through trial and error, in a learning process that demonstrates a certain incompatibility of the mental model based on traditional manufacturing with the modern resources of additive manufacturing. This incompatibility is noticed when, for example, a part manufactured in a 3D printer needs several subsequent treatments (e.g. removal of excessive supports, different machining, etc.), reducing the effectiveness of additive manufacturing, in addition to adding new costs. These post-treatments, their added costs and manufacturing time can be reduced through the use of design capabilities for additive manufacturing (Chakrabarti & Arora, 2019).

In the oil and gas industry, in many situations, operations at any stage of the production chain can be interrupted by the failure of an equipment, requiring the activation of its pair, in stand-by, and the immediate maintenance of the equipment now inoperative. However, several replacement items (spare parts) are difficult to supply quickly. This is the case of old equipment and machinery whose manufacturers no longer exist, the change of models (planned obsolescence), or the complexity and/or manufacturing time by traditional methods (e.g. machining, casting, forging, extrusion, etc.). This fact can greatly delay both preventive and corrective maintenance schedules (Inovação Industrial, 2021).

Another example of this fact is the unforeseen events that occur during scheduled shutdowns (e.g. in refineries, platforms, FPSOs, etc.), when equipment is opened and the maintenance team is faced with internal elements and/or deteriorated components, whose replacement was not foreseen during the planning of the shutdown. Therefore, the agility in the supply of certain spare parts is a strategic element within the industry. It so happens that from the identification of the necessary parts to their supply, precious time elapses in the acquisition and supply of these items, especially for complex replacement parts, as explained in the previous paragraph. Even opting for digital fabrication/3D printing of the necessary items, considerable time will still elapse for the identification of technical specifications, generation of drawings, modeling for digital fabrication, and 3D printing (Manufatura Digital, 2021).

2. MATERIALS AND METHODS

PH1, the material used in this work, is a precipitation hardenable martensitic stainless steel that has good corrosion resistance and excellent mechanical properties. It is used in a wide variety of applications, from medical prostheses to aerospace applications, when steels with high mechanical and corrosion resistance are required. In addition, PH1 structures can be subjected to various manufacturing processes such as machining, EDM, Micro Shot Peening (MSP), polishing and coating. The characteristics and mechanical properties of this steel, according to the manufacturer's information, are recorded in Table 1 (EOS GMBH, 2019).

Table 1. Composition of PH1 (EOS GMBH, 2019)

Element	Composition (% by mass)
Iron	Equivalent
Chrome	14 - 15.5
Nickel	3.5 - 5.5
Copper	2.5 - 4.5
Manganese	Max 1
Silicon	Max 1
Molybdenum	Max 0.5
Niobium	0.15 - 0.45
Carbon	Max 0.07

Solubilization heat treatment followed by aging, as described in ASTM specification A564, improves the properties of PH1. This treatment (H900) consists of heating the material to a temperature of 480 °C for one hour, followed by air cooling. Table 2 lists the values provided by the manufacturer.

Table 2. Mechanical properties of PH1 Stainless Steel (EOS GMBH, 2019), see Fig.1

Property	Without Heat Treatment	With Heat Treatment (H900)
Tensile Strength, Ultimate (XY)	1150 ± 50 MPa	1450 ± 100 MPa
Tensile Strength, Ultimate (Z)	1050 ± 50 MPa	1450 ± 100 MPa
Tensile Strength, Yield (XY)	1050 ± 50 MPa	1300 ± 100 MPa
Tensile Strength, Yield (Z)	1000 ± 50 MPa	1300 ± 100 MPa
Elongation (XY)	16% ± 4%	12% ± 2%
Elongation (Z)	17% ± 7%	12% ± 2%
Hardness	30 - 35 HRC	40 HRC

In this study, several specimens were manufactured by AM in different directions, to evaluate the possible anisotropy of the mechanical properties:

- Tensile: 4 specimens were manufactured in 3 different orientations, totaling 12 specimens;
- Impact: 12 specimens were manufactured in 2 different orientations, totaling 24 specimens;
- Hardness and roughness: 25 specimens were manufactured, distributed equally along the entire length of the printing table;

The manufacturing orientations considered are shown in Figure 1.

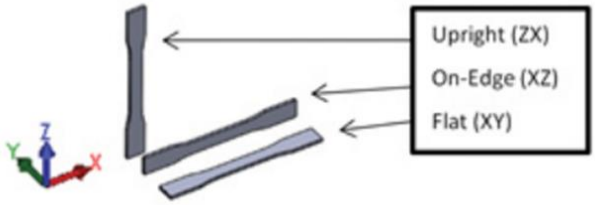

Figure 1. Possible parts construction orientations (Stratasys Ltd, 2021)

The tensile test, standardized by ASTM E8, aims to measure the strength and ductility of the material under uniaxial tensile stresses. These measurements can be used to compare materials, develop alloys, control quality, and design components. In this test, an Instron electromechanical machine model 5500R was used to perform the tensile tests, at the Mechanical Tests Laboratory (LEM) from the Technological Institute at PUC-Rio, ITUC. Four specimens were manufactured, following the Subsize Specimen specifications described in ASTM E8, in 3 different orientations, totaling 12 specimens. The orientations used were XY or flat, XZ or on-edge, and ZX or upright. This analysis is necessary because both in traditional and additive manufacturing, these modifications result in different mechanical properties.

In this study, both the roughness of the material and its variation with the position in which the part is manufactured were evaluated. The printing table has an area of 250 mm by 250 mm, and twenty-five units of equally spaced cubes were printed, as shown in Figure 2. Each cube was properly numbered. All roughness tests were performed at the Dimensional Metrology Laboratory (LMD) at PUC-Rio. The equipment used in the roughness tests was the Taylor-Hobson model Form Talysurf 50. The specimens analyzed in this test were the same used in the hardness test. The roughness was measured before the cubes were released from the printing table, and without carrying out the heat treatment. In addition, this procedure was performed in two moments: before and after shot peening with micro glass spheres.

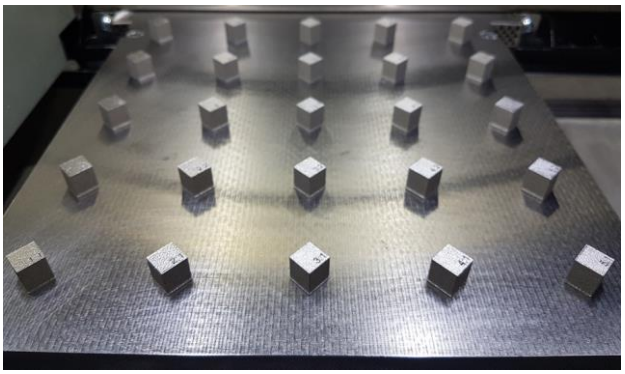

Figure 2. Printing of specimens for roughness and hardness evaluation

The specimens used in the hardness test were the same used previously in the roughness tests. However, in the hardness tests, the specimens had already been shot peened with micro glass spheres. With the 25 specimens tested, not only the hardness of the material was evaluated, but also its variation depending on its positioning on the 3D printer table. All hardness tests were performed at the LEM-ITUC. The machine used in these tests was the Wolpert DiaTronic. The method used in the test was the Vickers HV10 scale, with the application of 10 kgf of load. Measurements were taken on two sides (top and side) of each specimen.

In this study, twenty-four specimens were printed, following the specifications of the ASTM E23 standard, twelve of which were manufactured in the flat position and twelve in the on-edge position. The specimens were subjected to standard heat treatment after printing and the surfaces were polished, with the exception of the notch, which remained as built. All impact tests were carried out at the LEM-ITUC. The equipment used was the Instron model SI – 1K3 Charpy machine. It provides measurements of absorbed energy in two different units: joules (J), with an accuracy of 2 J, and foot-pound (ft.lb), with an accuracy of 1 ft.lb. For both flat and on-edge specimens, six temperature values were used to perform the measurements: -40, -20, ambient temperature, 100, 240 and 350 °C. Two specimens were tested in each of one of them.

The Scanning Electron Microscopy (SEM) images were performed using the Hitachi TM3000 Tabletop Microscope, located in the laboratory of the Department of Chemical and Materials Engineering at PUC-Rio. Images were obtained by SEM of the metallic powder with different amplifications, to observe the morphology and size distribution of the particles. The fracture surface of the impact specimens tested at different temperatures were also observed to characterize the fracture micro mechanism acting in each of the conditions studied.

3. RESULTS AND DISCUSSION

3.1 Scanning Electron Microscopy (SEM) analysis

In Figure 3, it can be seen that the PH1 powder has a spherical, rough shape and different sizes. Pal et al. (2016) also performed SEM analyzes of PH1, identifying similar characteristics, including specification of the powder particle diameter range, 5-30 µm.

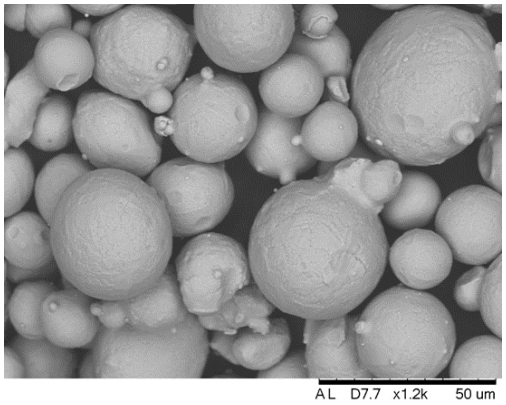

Figure 3. PH1 SEM image at x1.2k

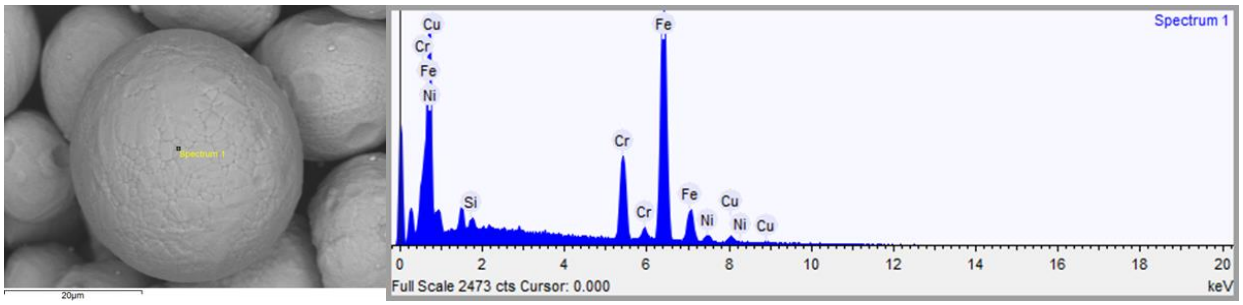

Figure 4. SEM image of PH1 analyzed in EDS and its spectrum

To qualitatively evaluate the chemical composition of PH1, some of the particles indicated in the images were analyzed by EDS, as shown in Figure 4. The composition identified does not consider the identified amount of carbon, due to the influence of the carbon tape used to fix the sample during the test. The elements identified in the measured spectrum are listed by the manufacturer in similar proportions, according to Table 1. Impurities with elements not foreseen by the manufacturer have not been identified.

3.2 Roughness tests

The specimens analyzed in this test were the same used later in the hardness tests. The roughness analysis was performed before the cubes were released from the printing table and their heat treatment. In all measurements made, the sampling length was approximately 1 mm. Table 3 summarizes the measured roughness.

Table 3. Comparison between the roughness parameters obtained from the cubes

Item	Ra (µm)	Rz (µm)	Rq (µm)	Rc (µm)
Lowest measured value	1.4970	7.8147	1.8384	5.4824
Highest measured value	4.4378	19.1980	5.5903	17.5909
Final media	2.8165	14.6289	3.7013	9.8208
Standard deviation	0.7061	3.0660	0.9001	2.7924
Standard error	0.1414	0.6132	0.1800	0.5585

Pal et al. (2016) analyzed the surface roughness of samples printed on the same material studied here, PH1 steel, obtaining a range of values for Ra between 9.39 and 10.90 µm. The values presented in Table 3 have a wide variation range, larger than that obtained by the authors of the aforementioned article. However, the highest value obtained for Ra is still about half of the lowest value obtained by the authors. Despite being the same material, this difference could be

due to a different printing machine, resulting in a different surface quality. Additionally, a comparative analysis of the printed cubes was carried out, a relationship was made between the surface roughness and the positioning of each cube on the printing table for each analyzed parameter, see Figure 5. It is possible to see a gradual increase in surface roughness in a diagonal direction from the upper right corner (Line 1, Column 5) to the lower left corner (Line 5, Column 1). The roughness of the specimen L1C5 is always the smallest or the second smallest, in this case only being larger than that of the element L1C1. The roughness of the specimen L1C3 is always the second highest, different from all the other elements around it. Based on this information and on the printing process, this fact indicates that the flow in that region is not fully operational, thus generating a larger accumulation of particles during the process, and consequently increasing its surface roughness. This may be due to equipment manufacturing problems, or lack of periodic maintenance. Also, using one of the peripherals of the 3D printing machine (EOS M280), a post-treatment was carried out on the printed parts, through a shot peening with glass spheres, whose blasting speeds and temperatures can be controlled. After peening, there was a reduction of up to about 70% of the previously measured roughness, even obtaining average Ra values close to 1 µm.

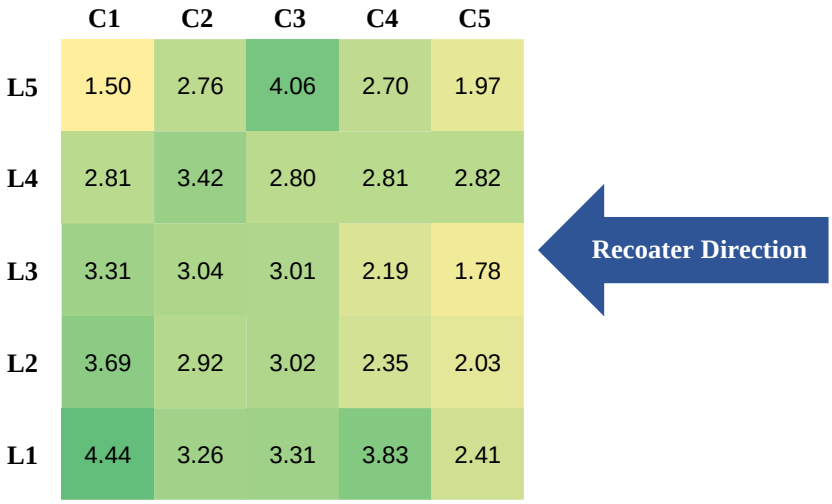

Figure 5. Ra values obtained from the specimens, according to their position on the printing table

3.3 Tensile tests

The DMLS process generates residual stresses in the printed parts, and to reduce them, a heat treatment is used after their manufacture. The printed parts need a support, and in the case of the tensile specimens the residual stress was able to separate the part from the support itself due to its length, see Figure 6.

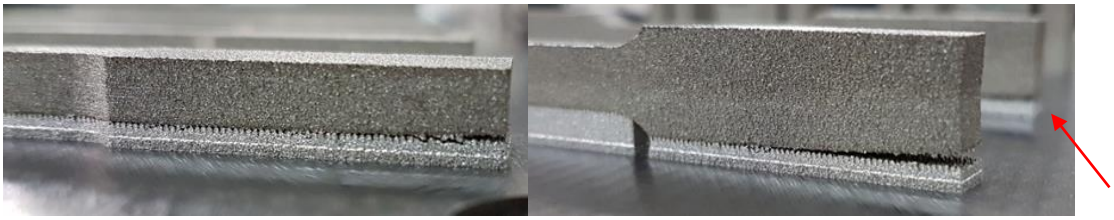

Figure 6. Flat and on-edge specimens, respectively, separated from their supports due to residual stress

In the on-edge specimen, the result of this support failure due to residual stresses is more visible. As this occurs in the middle of the manufacturing process, it is noted that the face close to the flaw (highlighted in the image by the red arrow) does not remain straight because during the process there is a change in the direction of the sintering layers. If the volume of the parts is too large, the resulting residual stress is even capable of deforming the construction table plate as identified by Prabhakar et al. (2015) in Figure 7. Therefore, changes were made to the 3D model to reinforce the ends of these specimens and prevent this failure from occurring, see Figure 8.

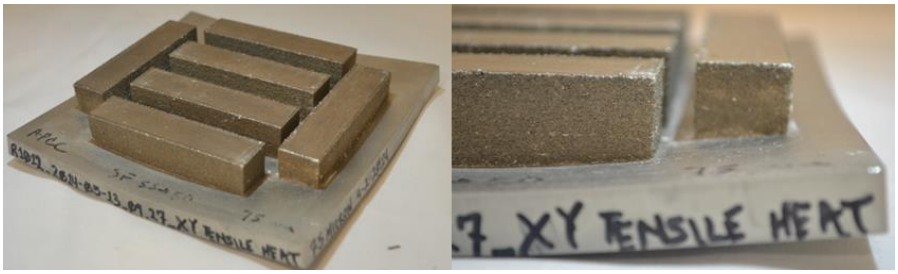

Figure 7. Deformation of the printing plate due to residual stresses (Prabhakar et al., 2015)

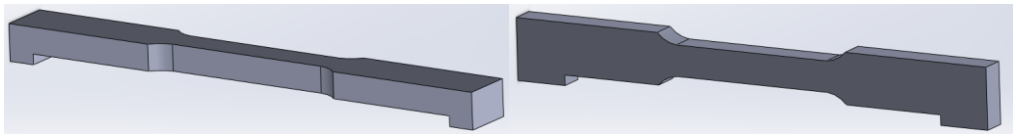

Figure 8. Modified three-dimensional model of the flat and on-edge specimen, respectively

After performing these modifications, the specimens for this test were manufactured in the three desired orientations with these modifications. They were then tested after being heat-treated. Four extra specimens were printed in the flat position without heat treatment and were tested as well. The results obtained were then compared with the heat-treated specimens (printed in the same position), see Figure 9(a). This figure shows that untreated specimens do not have a well-defined yield point and that their total strain is larger, so they are more ductile. Heat-treated specimens have higher yield and ultimate strengths, but lower overall strain, so they are less ductile. This difference is not necessarily due only to the heat treatment, but also to the residual stresses that were not relieved in the specimens due to the lack of heat treatment. For each remaining orientation, four specimens were tested, and the average of their engineering stress-strain curves are shown in Figure 9(b).

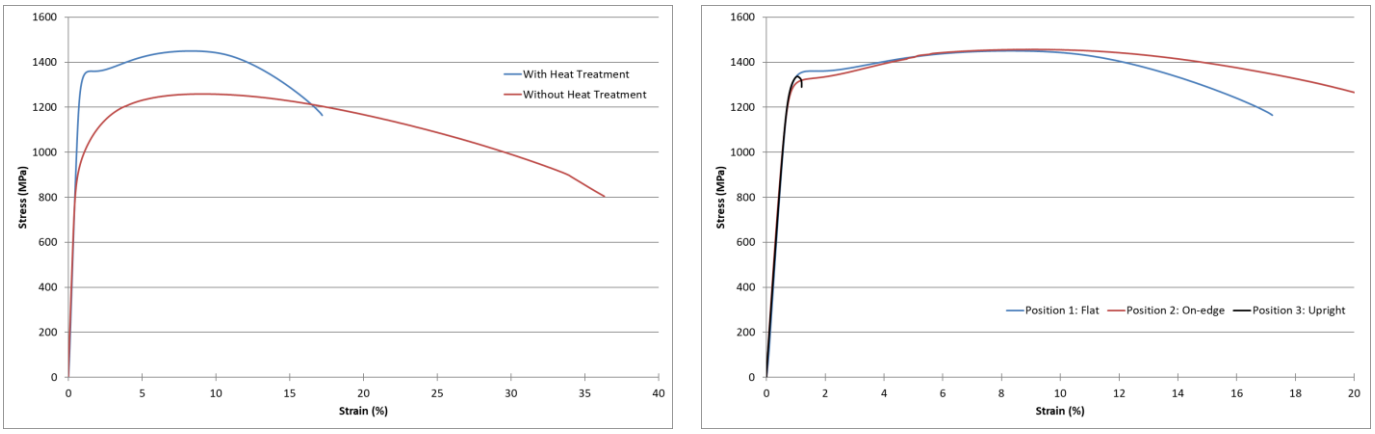

(a) (b)

Figure 9. Comparison of engineering stress-strain curves (a) between specimens with and without heat treatment and (b) between different orientations

It can be seen in Figure 9(b) that for Position 1 and Position 2 the graphics are very similar, with very close ultimate tensile values and a small difference in strain at rupture. However, the specimens printed in Position 3 practically did not undergo plastic deformation, with failure occurring close to the yield point. An in-depth analysis confirmed that the radius of the fillets of the specimens printed in the upright direction (vertical) were different, at one end the resulting impression radius was 5.18 mm while at the other the radius was 6.36 mm. It is believed that this difference resulted in a different stress concentration at each end, and that, therefore, failure occurred outside the central section, where it is normally observed. This situation demonstrates that parts manufactured with opposite concavities will probably not keep the same measure and depending on the final use, it will be necessary to carry out a machining to guarantee symmetry. Despite this, the results obtained for the other two positions exceed the values found for the similar material obtained through traditional manufacturing.

3.4 Hardness tests

To assess the possible anisotropy of the manufacturing process, the hardness was measured on two faces of each cube, the top face and the side face. On each face, three measurements were made and the average of them was considered as the hardness value of that cube on the face in question.

Table 4. Comparison between measurements made on the cube faces

Item	Face 1	Face 2
Lowest measured value	382	385
Highest measured value	417	418
Final media	400	398
Standard deviation	11.386	10.827
Standard error	2.2773	2.1653

The data in this table show that the hardness of the parts is almost isotropic, as both the total averages and the range of measured values for the two faces are very similar. According to the company's datasheet on this material, the minimum hardness value obtained must be 40 HRC, which is equivalent to about 388 HV, which is consistent with Table 4 measurements (EOS GMBH, 2019). Observing the values obtained, with their respective positions on the printing table, there is a small increase in the hardness of the columns close to the starting point of the recoater (blade that distributes the powder material in each layer); while there is practically no difference between the lines. It can be seen that the two faces have similar hardness, again proving the hardness isotropy of the manufacturing process.

To better analyze the difference in the values found, an image was created for all the specimens in their respective positions on the printing table, for the two sides measured.

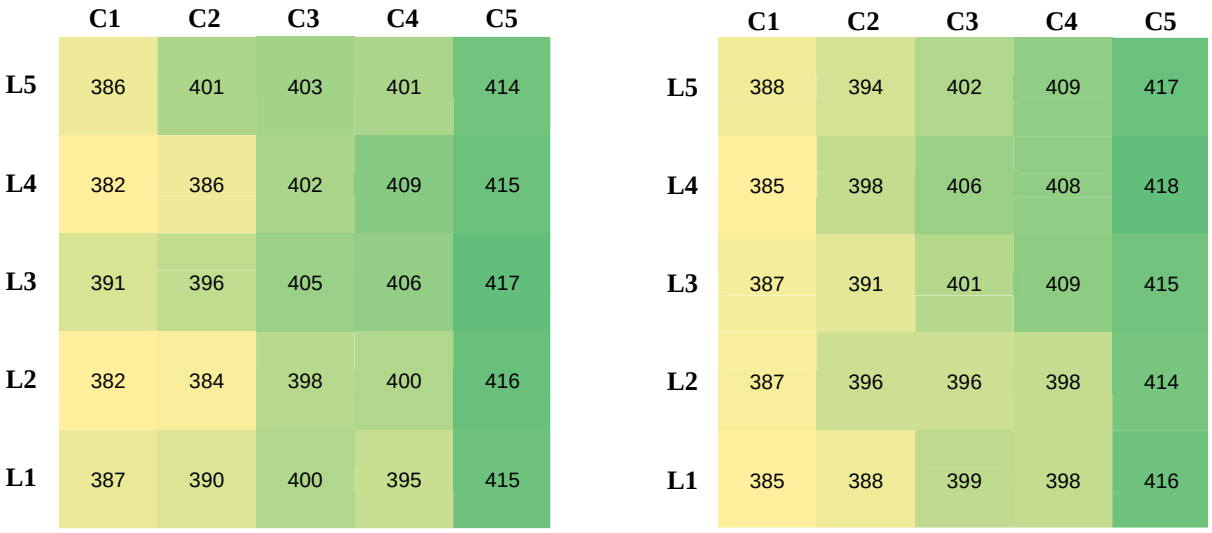

Figure 10. Average hardness values obtained on the (a) upper face of the specimens and (b) on the side face of the specimens, according to their position on the printing table

There is an increase in the values of the specimens close to the starting point of the recoater distribution. However, there is also an increase in the diagonal of the table, concentrating the highest values in the upper right corner. This can be seen again on both sides. This event can occur due to two main factors. First, during the printing process, the machine has a system of constant flow of inert gas, where on one side the gas is blown and on the other it is sucked in. During the sintering process, material remnants can spread across the rest of the print area on the table. This constant flow of inert gas occurs so that these remnants of material follow the flow of gas, and do not deposit on the surface of any other part present in the print. Thus, it is avoided that these remnants are trapped between the layers, possibly creating voids or other defects in the other parts. However, the pieces closer to the flow outlet can benefit more than those that are further away.

The second factor is related to the recoater. With each printing layer, the material tray located on the right side of the machine raises the layer height defined in the software previously, in this case 20 µm. The blade then moves from right to left to distribute this material from the tray evenly across the print table. However, it is believed that during the recoater movement the first part of the table (right side) receives the material of the new layer more evenly, while the end of the table can receive it unevenly or even have spaces that receive almost no material. With this, the chances of creating voids or other defects would be greater. Therefore, it is understood that this uneven material distribution is the cause of the results observed in the specimens, where the further right columns have values larger than those on the left.

3.5 Impact tests

Table 5 lists the temperature values of the tests and the energy absorbed by each specimen, in their respective orientations.

Table 5. Evaluated temperature values and energy absorbed obtained

Flat		On-edge	
Temperature (°C)	Absorbed energy (J)	Temperature (°C)	Absorbed energy (J)
- 49	0	- 39	18
- 45	0	- 38	20
- 19	0	- 19	26
- 20	0	- 20	26
28	12	28	38
28	8	28	34
100	48	100	42
98	44	102	44
238	46	243	48
239	34	240	50
350	34	320	42
349	40	325	42

There is a big difference between Table 5 and the results obtained for the similar laminated material on the market, UNS S15500 steel. The CVN value, at room temperature, of the UNS S15500 material in the H900 condition is 50 J/cm^2 (AK Steel Holdings Corporation, 2021), while the average value obtained for the flat specimens is 12.5 J/cm^2, a value within the range (10.85±1.20 J/cm^2) described by Sagar et al. (2017). For the on-edge specimens, the average was 45 J/cm^2. Both results are below the standard market value, and the difference for one of the types of specimens was only 10%. With this, it can be concluded initially that the positioning used during the manufacture of any part by DMLS has a greater influence than the difference in the manufacturing method (traditional or additive manufacturing). After this preliminary analysis of the CVN values, images of the fracture surfaces of the specimens were made for each temperature studied.

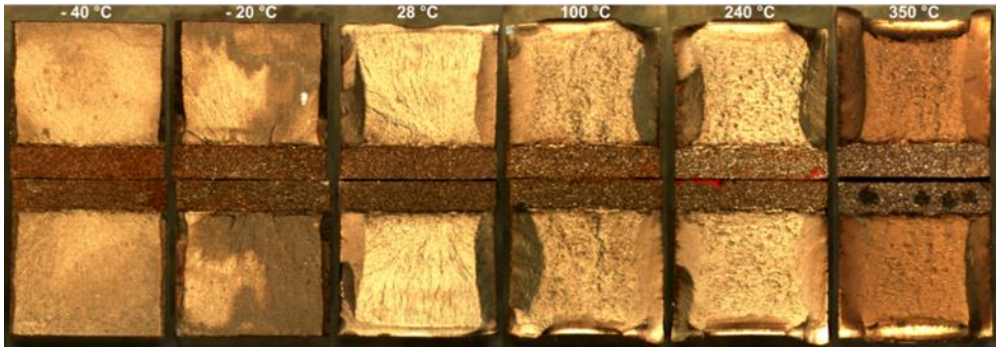

Figure 11. Image of the fracture surfaces of the on-edge specimens

In Figure 11, both the beginning of the ductile-brittle transition and the percentage of shear lip (PSF) present on the surfaces can be evaluated. However, it was not possible to identify the temperature range where the transition begins, since the specimen tested at – 40 °C already has a small percentage of ductile fracture, indicating that the transition at this temperature has already begun. Thus, what can be said is that the transition occurs at a temperature below –40 °C, while at the temperature of 100 °C the percentage of brittle fracture is still higher than the ductile one on the surfaces of the image. To confirm this analysis, it is necessary to study the ductile-brittle transition graph of the material. To obtain it, MATLAB (based on the Levenberg–Marquardt algorithm) and the theory of Oldfield (1979), were used.

Analyzing the curve of the Flat-type specimens, the upper threshold is 41 J while the average transition temperature is approximately 30 °C. Thus, it is observed that even at positive temperatures, completely brittle fractures can occur. For the on-edge specimens, the upper energy level is 45 J, while for these specimens; the average transition temperature is approximately equal to – 28 °C. With this, there is a large difference between the different specimens, because only at negative temperatures will completely brittle fractures occur in the on-edge specimens. The difference between the upper levels is not so great (4 J), so at high temperatures the behavior of the two types of specimens is similar. However, what most differs one curve from the other is the transition range. For Flat specimens, this range is very short, so if the fracture surfaces analyzed in Figure 11 were from this test, a jump in shear lip percentage would be observed. While for the on-edge specimens, due to the large transition range, the percentage can be observed gradually increasing as the temperature increases. In this way, estimating the beginning of the transition range through the analysis of fracture surfaces also becomes easier. These results clearly indicate that anisotropy is a major issue in the toughness of the printed PH1 steel.

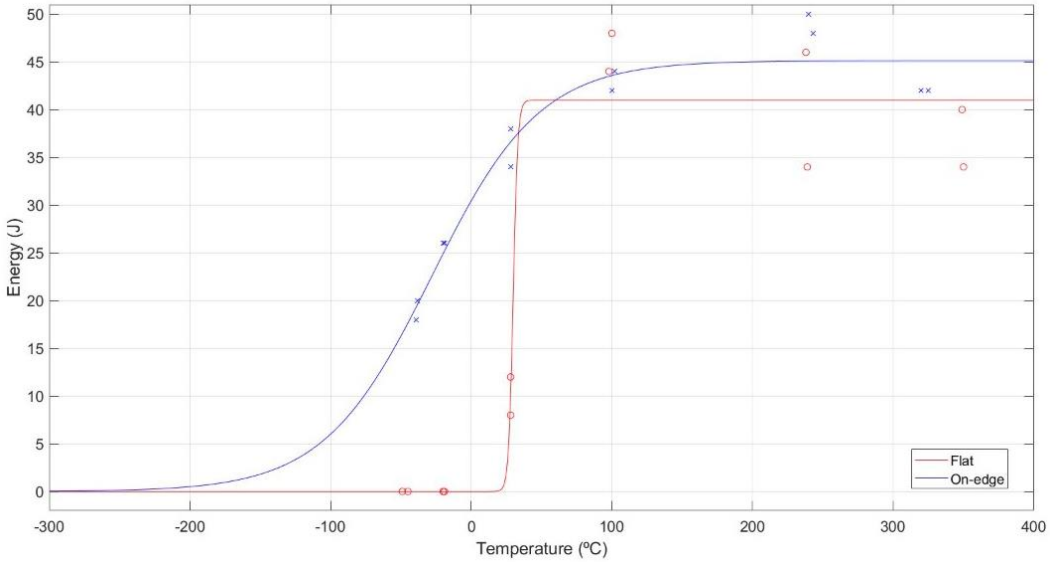

Figure 12. Comparative analysis between the two ductile-brittle transition curves

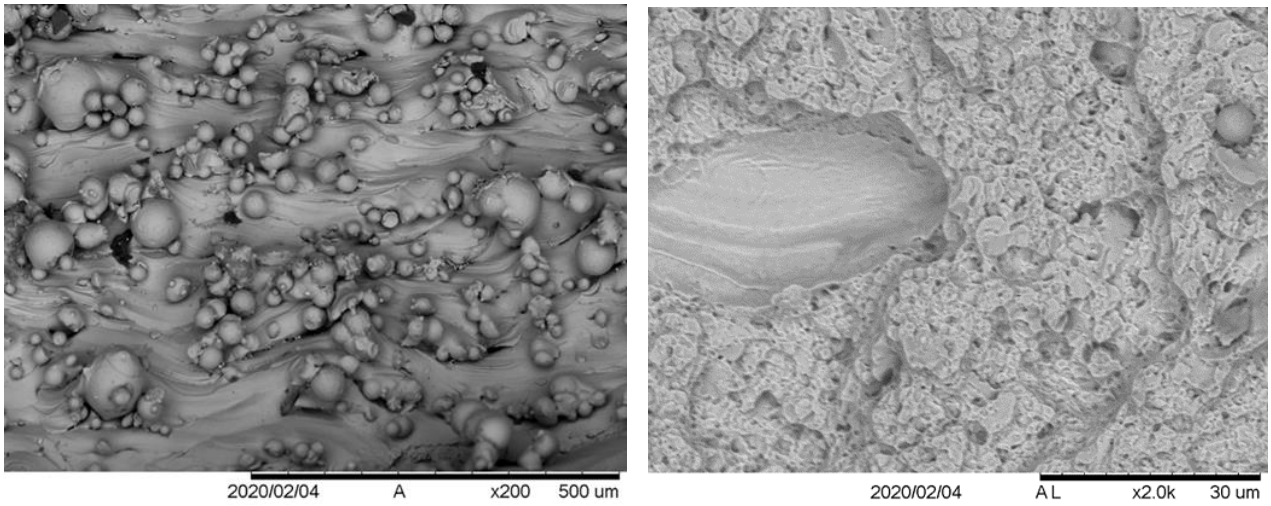

(a) (b)

Figure 13. (a) Specimen notch surface printed in on-edge position after impact test and (b) specimen surface printed in flat position after impact test at - 40 °C

The images bellow were taken from the fracture surfaces of the test specimens from the impact test. Initially, an image of the notch surface of the specimen was made, see Figure 13(a). The surface is relatively flat, with irregularly shaped voids, and apparent layers and undulations along the entire surface, with the presence of particles of different sizes and mostly spherical in appearance. These particles are possibly the metallic powder that was not melted during the laser sintering process, as also identified by Ladani & Sadegilaridjani (2021), Zitell et al. (2019), and Liverani et al. (2017). Layers and ripples are similar to those found by Liverani et al. (2017), in 316L steel manufactured by DMLS, where it identifies as molten metal regions. Figure 13(b) shows the surface of the printed specimen in the flat position after impact testing at - 40 °C. It is possible to observe that the surface is quite porous, with the presence of some spherical shaped elements, as identified in other SEM images, in addition to the presence of void. Liverani et al. (2017) identified voids in samples of 316L manufactured by DMLS as gas pores. It was not possible to observe any characteristic micromechanism in the sample, but the general appearance of the surface indicates the presence of brittle fracture facets characterized by smooth surfaces.

4. CONCLUSION

After analyzing the set of tests performed, it was concluded that it is possible to use parts manufactured through DMLS to replace parts obtained through traditional manufacturing. However, for this, certain reservations are necessary because the printing orientation directly influences the intrinsic properties of the material. As previously described, there is a big difference in the mechanical behavior of the parts when they go through the heat treatment process or not. In

addition, the analysis with different orientations indicated that pieces printed in the upright position are fragile and that, in this case, pieces printed in the flat and on-edge positions have similar and better behaviors than that found for similar material obtained traditionally.

However, this does not occur in the impact test, where the results for the two orientations (flat and on-edge) were different. In one of the orientations (on-edge), the values found were similar to what is traditionally found, while the specimens of the other orientation (flat) were well below, comparatively. The images made of these specimens in the SEM indicate that there are elements that are most likely grains that were not properly sintered during production and this may be one of the reasons for the fragility of the material.

Additionally, with the hardness and roughness tests, it was observed that there is a difference in the final result of the production of a part depending on its positioning on the printing table. This may be a feature of the EOS company's process or equipment.

It is concluded that it is necessary to consider that there are still limitations in this technology, such as what happened with the tensile test specimens that were printed vertically. It was observed that the machine was not able to maintain the radius predicted by the three-dimensional file and thus failed unexpectedly.

Despite these considerations, the final part obtained has good mechanical properties, at times even surpassing the properties of the original material (UNS S15500) as in the tensile tests.

5. REFERENCES

AK Steel Holdings Corporation, 2018. Product data sheet 15-5 PH Stainless Steel. 09 Apr. 2021. <https://www.spacematdb.com/spacemat/manudatasheets/15-5_PH_Data_Sheet.pdf > Acessado em: abril de 2021.

American Society For Testing And Material - ASTM. E 23, 2007. Standard Test Methods for Notched Bar Impact Testing of Metallic Materials.

American Society For Testing And Material – ASTM. E 606, 2019. Standard Test Method for Strain-Controlled Fatigue Testing.

American Society For Testing And Material - ASTM. E 8, 2013. Standard Test Methods for Tension Testing of Metallic Materials.

Bosh, 2021. Indústria 4.0: muito além da automação. 12 Jul. 2021. <https://www.bosch.com.br › industria-4-0>.

Chakrabarti, A.; Arora, M., 2019. *Industry 4.0 and Advanced Manufacturing*. 1st ed. Springer Singapore.

EOS GMBH, 2019. PH1 datasheet. 18 Dec. 2019. <https://gpiprototype.com/pdf/EOS-StainlessSteel-PH1.pdf>

Inovação Industrial, 2021. Indústria de óleo e gás 4.0: o que muda no setor?. 20 Dec. 2021. <https://inovacaoindustrial.com.br/industria-de-oleo-e-gas/>.

Ladani, L.; Sadeghilaridjani, M., 2021. Review of Powder Bed Fusion Additive Manufacturing for Metals. *Metals*, v. 11, p. 1391. Doi: 10.3390/met11091391.

Liverani, E. et al.,2017. Effect of selective laser melting (SLM) process parameters on microstructure and mechanical properties of 316L austenitic stainless steel. *Journal of Materials Processing Technology*, v. 249, p. 255–263.

Manufatura Digital, 2021. Desenvolvimentos da Impressão 3D na Petrobras. 21 Dec. 2021: <https://www.manufaturadigital.com/desenvolvimento-impressao-3d-petrobras/>.

Oldfield, W., 1979. Fitting Curves to Toughness Data. *Journal of Testing and Evaluation*, p. 326-333.

Pal, S. et al., 2016. The Effect of Post-processing and Machining Process Parameters on Properties of Stainless Steel PH1 Product Produced by Direct Metal Laser Sintering. *Procedia Engineering*, v. 149, p 359-365. 10.1016/j.proeng.2016.06.679.

Prabhakar, P. et al., 2015. Computational Modeling of Residual Stress Formation during the Electron Beam Melting Process for Inconel 718. *Additive Manufacturing*, v. 7, p. 83-91.

Sagar, S., et al., 2017. Room-Temperature Charpy Impact Property of 3D-Printed 15-5 Stainless Steel. *Journal of Materials Engineering and Performance*, v. 27, p. 52–56.

Stratasys Ltd, 2017. Stratasys FDM Nylon6 datasheet. 07 May 2021. < https://www.stratasys.com/siteassets/materials/materials-catalog/fdm-materials/nylon-6/mss_fdm_nylon6_1117a.pdf?v=48da60 >

Zitelli, C., Folgarait, P., Schino, A., 2019. Laser Powder Bed Fusion of Stainless Steel Grades: A Review. *Metals*. 9. 731. 10.3390/met9070731.

6. RESPONSIBILITY NOTICE

The authors are the only responsible for the printed material included in this paper.